The Journal of Experimental Biology 213, 408-417

doi:10.1242/jeb.031914

Approaching the evolutionary advantage of ancillary types of haemoglobin in *Daphnia magna* by simulation of oxygen supply

S. Moenickes[1], O. Richter[1] and R. Pirow[2,*]

[1]Institute of Geoecology, Technical University of Braunschweig, Germany and [2]Institute of Zoophysiology, University of Münster, Germany

*Author for correspondence (pirow@uni-muenster.de)

Accepted 16 October 2009

SUMMARY

The planktonic crustacean *Daphnia magna* synthesizes haemoglobin (Hb) macromolecules of variant subunit composition and oxygen affinity. This is one of the strategies by which the animals cope with variations in environmental conditions such as ambient oxygen tension. The enrichment of high-affinity Hb molecules in the haemolymph of hypoxia-exposed animals is thought to reduce Hb synthesis costs due to an enhanced transport efficiency of these molecules in comparison to the low-affinity Hb molecules. How great this economic advantage is, and under which conditions this benefit disappears, is still not fully understood. Here we implemented a rigorously simplified model of the daphnid body and described the transport of oxygen from the environment *via* the haemolymph to the tissues in terms of the convection–diffusion–reaction equation. The model was validated by comparing various model predictions with experimental data. A sensitivity analysis was used to evaluate the influence of parameter uncertainties on the model predictions. Cost–benefit analysis revealed in which way at the system's level the increase in Hb oxygen affinity improves the oxygen loading at the respiratory surfaces and impairs the release of oxygen to the tissues. The benefit arising from the improved oxygen loading exceeds the disadvantage of impaired unloading only under conditions where the ambient oxygen tension is critically low and the Hb concentration is high. The low-affinity Hb, on the other hand, provides an advantage given that the Hb concentration is low and the ambient oxygen tension is well above the critical level. Computer-aided modelling and simulation therefore provide valuable mechanistic insights into the driving forces that could have shaped the evolution of globin genes in daphnids.

Key words: oxygen transport, computer modelling, simulation, haemoglobin, respiration, circulation, *Daphnia*, Crustacea.

INTRODUCTION

One of the challenges of organismic biology is to understand how genes, proteins, cells, tissues and organs operate synergistically at different levels of biological organization to establish a stable internal milieu under varying physiological and environmental conditions. Owing to the hierarchical structure and dynamic properties of biological homeostatic systems, it is generally difficult to predict, in a quantitative manner, how adjustments in individual components affect the system behaviour as a whole. Such quantitative predictions can be important for testing hypotheses on the benefit of the animal's molecular responses to environmental stress.

In the present paper, we used computer-aided modelling and simulation to analyse the consequences of gene expression-mediated adjustments in the haemoglobin (Hb) of the planktonic crustacean *Daphnia magna* Strauss 1820. Among the daphnids, which play an important role in ecological research, toxicology and environmental monitoring, and in the emerging fields of ecological and toxicological genomics (Poynton et al., 2007; Eads et al., 2008; Heckmann et al., 2008; Shaw et al., 2008), the euryoxic species *D. magna* stands out due to the striking induction of Hb synthesis upon exposure to environmental oxygen deficiency (Fox, 1948; Fox et al., 1951; Kobayashi and Hoshi, 1982; Tokishita et al., 1997; Zeis et al., 2003; Gorr et al., 2004). The hypoxic induction of Hb synthesis is associated with a differing expression of globin genes, giving rise to macromolecules of altered subunit composition and enhanced oxygen affinity (Kobayashi et al., 1988; Kobayashi et al., 1994; Kimura et al., 1999; Zeis et al., 2003; Gorr et al., 2004; Lamkemeyer et al., 2005). Remarkably, this kind of intrinsic molecular adaptability is not restricted to *Daphnia* Hb but has also been found in the haemocyanin of a decapod crustacean (deFur et al., 1990). The Hb macromolecules of *D. magna* are large-sized 590 kDa proteins which are composed of 16 di-domain subunits (Lamkemeyer et al., 2006). Seven different subunit species (designated A–G) were identified by two-dimensional gel electrophoresis (Kimura et al., 1999; Zeis et al., 2003; Lamkemeyer et al., 2005). Four subunit types (B, C, E, F) are shared by the macromolecular isoforms isolated from normoxia-acclimated and hypoxia-acclimated animals (Zeis et al., 2003; Lamkemeyer et al., 2005). Subunit G is specifically expressed under normoxic to hyperoxic conditions, whereas subunits A and D become induced under hypoxic conditions. The induction of the last two subunits, and the shifts involved in the macromolecular proportions of the four constitutively expressed subunits, are implicated in the elevation of oxygen affinity in the Hb of hypoxia-acclimated animals (Zeis et al., 2003; Lamkemeyer et al., 2005).

The application of high-affinity Hb at the molecular level is thought to reduce Hb synthesis costs at the whole-animal level due to the enhanced transport efficiency (Kobayashi et al., 1994; Paul et al., 2004). How great this economic advantage actually is, and under which environmental conditions and physiological states this benefit disappears, is still poorly understood. Based on a broad spectrum of experimental data on the oxygen-transport physiology of *D. magna* (Paul et al., 1997; Pirow et al., 2004; Seidl et al., 2005),

we established a mathematical model that allowed us to quantify the advantages and disadvantages related to the low-affinity and high-affinity Hb. First, we describe the conceptual model, especially the geometric and parametric aspects, and their interdependency. Two different sets of parameters were employed to simulate the oxygen transport in both normoxia-acclimated and hypoxia-acclimated animals. For the normoxia-acclimated animals, we used a low Hb concentration (C_{Hb}) of 0.1 mmol l^{-1} haem (Zeis et al., 2003; Seidl et al., 2005) and a low-affinity equilibrium curve with a half-saturation oxygen tension (P_{50}) of 1.01 kPa (Kobayashi et al., 1994). For the hypoxia-acclimated animals, a five-fold higher C_{Hb} and a high-affinity equilibrium curve (P_{50}=0.35 kPa) were used. For model validation, we compared the case-specific predictions concerning (i) the dependence of oxygen consumption rate on inspiratory oxygen tension (P_i), (ii) the contribution of Hb to circulatory oxygen transport, and (iii) the spatial oxygen partial pressure distribution with experimental data. A sensitivity analysis was then performed to show how uncertainties in model parameters translate into variations in model prediction. A cost–benefit analysis was finally accomplished to scale the respective advantages of the low-affinity and high-affinity Hb types.

MATERIALS AND METHODS

The constitutive processes of oxygen transport in the tiny crustacean *D. magna* can be described by a well-known partial differential equation. Its realistic parameterization, however, strongly depends on the geometric model of the animal. We therefore start this section with a detailed description of both the process model and the geometric model before explaining the parameterization.

Process model

The mass balance equation for oxygen supply takes into account diffusive fluxes, convective fluxes, and consumption according to Michaelis–Menten kinetics:

$$\beta\frac{\partial P}{\partial t} = \nabla(K\nabla P) - \mathbf{v}\beta\nabla P - \frac{a_{max}P}{P_{50r}+P}\ , \qquad (1)$$

where P (kPa) is the oxygen partial pressure, β (nmol mm^{-3} kPa^{-1}) is the capacitance coefficient for oxygen, K (nmol s^{-1} mm^{-1} kPa^{-1}) is the Krogh constant for oxygen diffusion, $\mathbf{v}$ (mm s^{-1}) represents the fluid's vectorial velocity in the radial (r, mm) and axial (h, mm) direction, a_{max} (nmol mm^{-3} s^{-1}) is the maximum consumption rate under unlimited conditions and P_{50r} (kPa) is the oxygen partial pressure for half-maximum respiration.

The capacitance coefficient β and the Krogh constant K take into account the fact that molecular oxygen may occur in two mobile forms; namely as physically dissolved and Hb-bound species:

$$\beta = \alpha + C_{Hb}\frac{\partial S}{\partial P} \qquad (2)$$

and

$$K = D\alpha + D_{Hb}C_{Hb}\frac{\partial S}{\partial P}\ , \qquad (3)$$

where α (nmol mm^{-3} kPa^{-1}) is the physical solubility for oxygen, D and D_{Hb} (mm^2 s^{-1}) represent the diffusion coefficients for oxygen and Hb, respectively, and C_{Hb} (nmol mm^{-3}) and S (–) refer to the haem-based concentration and fractional oxygen saturation of Hb, respectively.

The reversible binding of oxygen to Hb is described by the Adair equation (Imai, 1982), which supposes that equilibrium is reached instantaneously between the two mobile forms. The fractional saturation S of a multimeric Hb with N interacting oxygen-binding sites is given by:

$$S = \frac{1}{N}\frac{P}{B}\frac{\partial B}{\partial P} \qquad (4)$$

and

$$B = 1 + \sum_{i=1}^{N}\binom{N}{i}P^i\prod_{j=1}^{i}K_j\ , \qquad (5)$$

where B is the binding polynomial for the Adair equation and K_j (kPa^{-1}) denotes the intrinsic association equilibrium ('Adair') constant for the jth binding step.

Topological model

The complex body of *D. magna* (Fig. 1A) is at first reduced to physiologically relevant parts, omitting morphological details such as limbs, head, etc. The remaining structure, consisting of strands of tissue, a haemolymph circuit with a heart, the respiratory medium, and the integument as the medium–haemolymph interface, is further rigorously simplified to a rotationally symmetric cylinder (Fig. 1B) which, however, may still be seen as an improvement on former models (Pirow, 2003; Pirow and Buchen, 2004). The animal's body is conceived as a cylindrical trunk which is wrapped by a hollow cylinder representing the carapace. The carapace is a double-walled, hollow structure that is perfused with haemolymph. The trunk is assumed to be further separated into alternating concentric layers of tissue and haemolymph. The space between the carapace and the trunk, also showing the shape of a hollow cylinder, is occupied by the respiratory medium.

Thanks to the symmetry of rotation, the model described so far may be reduced to a two-dimensional series of rectangular compartments (Fig. 1C). What is missing is a closed haemolymph circuit. We assume that no processes other than perfect mixing of haemolymph occur at the confluence points at the two ends of the model. Consequently, omission of the outflow–inflow interconnections is tolerable if we express this mixing and re-entrance by other means, e.g. by a set of boundary conditions. The oxygen partial pressure of the mixed haemolymph entering the trunk at the posterior and anterior ends (Fig. 1B) is defined as 'arterial' oxygen tension (P_a) and 'venous' oxygen tension (P_v), respectively. The values for P_a and P_v are derived from the mean oxygen concentration of the haemolymph leaving the respective confluence point. The latter is obtained by dividing the overall convective oxygen flow rate at the outflow boundaries by the overall haemolymph flow rate. Across one single outflow boundary the convective oxygen flow rate $\dot{M}$ (nmol s^{-1}) and haemolymph flow rate $\dot{Q}$ (mm^3 s^{-1}) are given by:

$$\dot{M} = \int_{r_i}^{r_o}\beta P v 2\pi r\,dr \qquad (6)$$

and

$$\dot{Q} = \int_{r_i}^{r_o} v 2\pi r\,dr\ , \qquad (7)$$

with r_i and r_o representing the inner and outer radii of the boundary line. All remaining boundaries are isolated except for the inflow and outflow of the respiratory medium. At the medium inflow the boundary condition is set to the inspiratory oxygen tension, at the medium outflow it is defined by convective flow only.

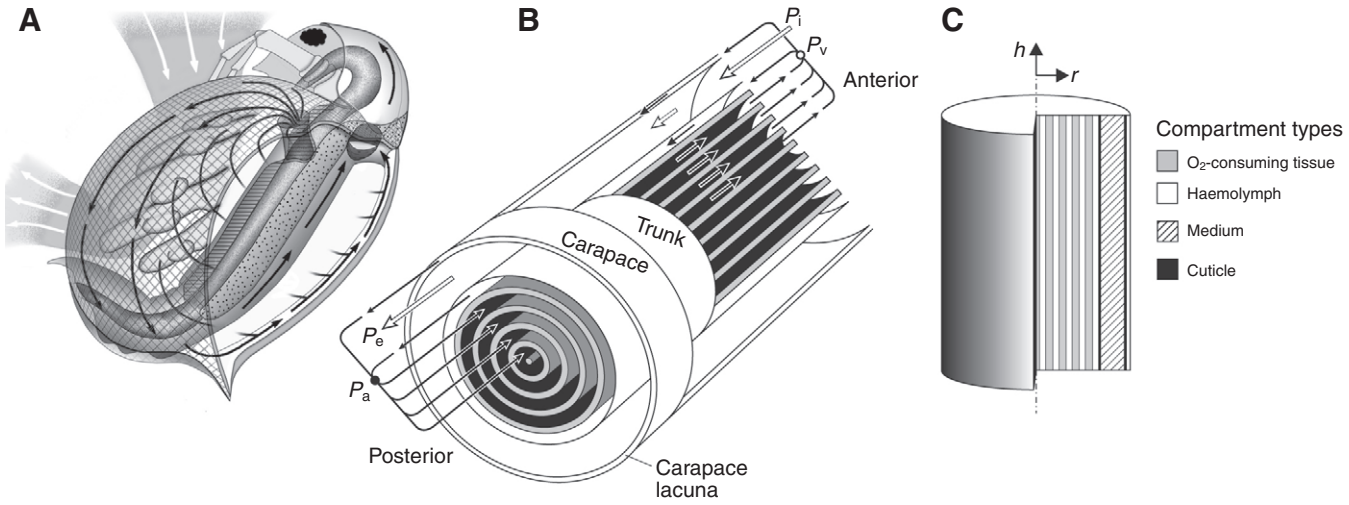

Fig. 1. (A) Dorsal view of *Daphnia magna* showing the medium flow pattern (white arrows) and the haemolymph flow pattern (black arrows) (Pirow et al., 1999a; Pirow and Buchen, 2004). A dorsal piece of the left carapace valve (grid area) was removed. (B) Topological model for oxygen transport in *Daphnia* based on a cylinder-within-tubes arrangement. Parts of the model are cut away to show the distribution of tissue compartments in the form of grey-shaded hollow and solid cylinders. Black and white arrows depict the flow of medium and haemolymph, respectively. P_i and P_e, inspiratory and expiratory oxygen tension, respectively; P_a and P_v, 'arterial' and 'venous' oxygen tension of the haemolymph entering and leaving the trunk, respectively. (C) Half-median plane of the radially symmetric model showing the succession of different compartment types. The axial and radial coordinates are indicated by *h* and *r*.

Geometric model

The number and geometrical extensions of the model compartments (Table 1) were derived from the following constraints. (1) The volume of the cylindrical model is 1.12 mm^3 and refers to a 2.5 mm long *D. magna* (Kobayashi, 1983); this volume includes the haemolymph and tissue compartments but excludes the medium and the cuticle compartment. (2) The tissue fraction of body volume is 0.4 (Kobayashi, 1983). (3) The cuticular layers covering the trunk and the inner side of the carapace are assumed to have a thickness of 0.002 mm and 0.001 mm (Pirow et al., 1999a), respectively. (4) The medium flows through a cross-sectional area of 0.4 mm^2 (Pirow and Buchen, 2004). (5) Tissue layers have a thickness of 0.04 mm; this figure represents an estimate of the average thickness of *Daphnia* muscles and was derived from anatomical drawings (Binder, 1932) and histological sections (Fryer, 1991). (6) All haemolymph layers in the trunk have the same thickness. (7) Haemolymph flow in identical directions shows identical velocity. The branching of total haemolymph flow into subcircuits obeys the conservation of mass. The height of the cylindrical model was chosen to be 2.38 mm, which is somewhat shorter than the length of a 2.5 mm *Daphnia* but ensured consistency with the constraints.

Table 1. Model geometry

Parameter	Value	Unit
Number of tissue compartments	5	
Thickness		
Tissue layers	0.040	mm
Haemolymph layers in the trunk	0.035	mm
Haemolymph layer in the carapace	0.023	mm
Cuticle of the trunk	0.002	mm
Cuticle of the carapace	0.001	mm
Medium compartment	0.148	mm
Trunk radius (including cuticle)	0.357	mm
Outer carapace radius	0.529	mm
Height	2.380	mm

Parameterization

The balance equation (Eqn 1) is valid in the whole animal. However, not all processes take place in all of its compartments. This is taken into account by locally parameterizing the balance equation. Consumption of oxygen takes place in the tissue compartments only, while Hb-mediated oxygen transport takes places in the haemolymph compartments only. Convection takes place in the haemolymph and the medium. The coefficient of radial and axial diffusion of dissolved oxygen generally depends on the medium considered, which comes down to their compartment-wise definition.

All parameter values refer to 20°C and are listed in Table 2. Compartment-specific diffusion coefficients for oxygen in tissue (D_T), haemolymph (D_H), and medium (D_M) were taken from the compilation given in Pirow and Buchen (Pirow and Buchen, 2004). The diffusion coefficient for oxygen in the cuticle (D_C) was derived by dividing the Krogh constant for the diffusion of oxygen in chitin [1.27×10^{-6} nmol s^{-1} cm^{-1} Torr^{-1} (Krogh, 1919)] by the chosen solubility of oxygen. The solubility of oxygen (α) was set to be alike in all compartments and equal to that of water (0.014 nmol mm^{-3} kPa^{-1}) (Forstner and Gnaiger, 1983). This value is a reasonable choice for the haemolymph and tissue compartments, since the oxygen solubility is only 10% lower in body fluids such as human plasma (58–85 g protein l^{-1}) and somewhat uncertain for the tissue compartment due to the range of reported values (±30%) for different tissue types [for details and references, see Pirow and Buchen (Pirow and Buchen, 2004)]. The diffusion coefficient of *D. magna* Hb (D_{Hb}) was assumed to be equal to that of the *Moina macrocopa* Hb (Sugano and Hoshi, 1971).

The flow velocities of medium and haemolymph are derived from the maximum appendage beating rate (340 min^{-1}) and heart rate (370 min^{-1}) of a fasting *D. magna* (body length: 2.5 mm, carapace length: 2.11 mm) without eggs in the brood chamber [see figure 7C,F of Seidl et al. (Seidl et al., 2005)]. The fluid flow direction in the medium and haemolymph compartments is considered to be

Table 2. Parameters of the model

Symbol	Value	Unit	Description
D_T	0.0010	$mm^2 s^{-1}$	Diffusion coefficient for O_2 in tissue
D_H	0.0015	$mm^2 s^{-1}$	Diffusion coefficient for O_2 in haemolymph
D_M	0.0020	$mm^2 s^{-1}$	Diffusion coefficient for O_2 in medium
D_C	0.00007	$mm^2 s^{-1}$	Diffusion coefficient for O_2 in cuticle
D_{Hb}	26×10^{-6}	$mm^2 s^{-1}$	Diffusion coefficient for Hb in haemolymph
α_T	0.014	$nmol\,mm^{-3}\,kPa^{-1}$	Solubility coefficient for O_2 in tissue
α_H	0.014	$nmol\,mm^{-3}\,kPa^{-1}$	Solubility coefficient for O_2 in haemolymph
α_M	0.014	$nmol\,mm^{-3}\,kPa^{-1}$	Solubility coefficient for O_2 in medium
α_C	0.014	$nmol\,mm^{-3}\,kPa^{-1}$	Solubility coefficient for O_2 in cuticle
v_b	0.3107	$mm\,s^{-1}$	Haemolymph flow velocity, backward direction
v_f	0.2752	$mm\,s^{-1}$	Haemolymph flow velocity, forward direction
v_M	1.8	$mm\,s^{-1}$	Medium flow velocity
C_{Hb}	0.1–0.5	$nmol\,mm^{-3}$	Haem-based Hb concentration
$S(P)$	See Fig. 5		O_2 equilibrium curve
a_{max}	0.016	$nmol\,s^{-1}\,mm^{-3}$	O_2 consumption rate of tissue
P_{50r}	0.02	kPa	O_2 tension for half-maximum respiration

Data refer to 20°C.

perfectly axial and, in particular, spatially constant per compartment; that is, fluid boundary layers are neglected (plug-flow). The axial medium flow velocity (v_M) is the quotient of medium flow rate and flow cross-sectional area; the medium flow rate was derived from appendage beating rate according to a functional relationship [see figure 7 of Pirow et al. (Pirow et al., 1999b)]. The haemolymph flow velocities in the backward (anterior-to-posterior) direction (v_b) and forward direction (v_f) are calculated from total perfusion rate which, equalling cardiac output, was obtained from heart rate and stroke volume (6.6 nl) [see figure 5 of Seidl et al. (Seidl et al., 2005)].

Two different sets of Hb-related parameters were employed to simulate the oxygen transport in the normoxia-acclimated and hypoxia-acclimated animals. For the normoxia-acclimated case, we used a low Hb concentration (C_{Hb}) of 0.1 nmol haem mm^{-3} (Zeis et al., 2003; Seidl et al., 2005) and a set of low-affinity Adair constants ($K_{1–8}$: 0.1, 0.1, 0.1, 0.1, 0.15, 0.15, 0.15 and 1.55 $mmHg^{-1}$) (Kobayashi et al., 1994). This is referred to as the Hb-poor low-affinity (PL) case. A five-fold higher C_{Hb} and a set of high-affinity Adair constants ($K_{1–8}$: 0.089, 0.23, 0.26, 0.38, 0.39, 0.51, 0.45 and 3.53 $mmHg^{-1}$) were chosen for the hypoxia-acclimated case, which is referred to as the Hb-rich high-affinity (RH) case. The different sets of Adair constants correspond to half-saturation oxygen tensions (P_{50}) of 1.01 kPa (PL case) and 0.35 kPa (RH case).

The volume-specific oxygen consumption rate (a_{max}) of pure tissue was calculated from the dry mass-specific consumption rate (268 $nmol\,h^{-1}\,mg^{-1}$) of a fasting, normoxia-acclimated *D. magna* [table 1 of Seidl et al. (Seidl et al., 2005)], taking into account the animal's body volume (1.12 mm^3), dry mass (0.096 mg) and tissue fraction (0.4) (Kobayashi, 1983). Metabolic differences between normoxia-acclimated and hypoxia-acclimated animals were neglected, and the value for a_{max} was assumed to be the same for the PL and the RH case. The oxygen partial pressure for half-maximum respiration (P_{50r}) in tissue of *D. magna* has not been determined yet. Reported values for isolated mitochondria from rat liver and brine shrimp embryos range from 0.025 kPa to 0.057 kPa at 25°C and state 4 respiration (Gnaiger et al., 1995; Gnaiger et al., 1998; Gnaiger et al., 2000). For our simulations in the 20°C condition, we chose a P_{50r} of 0.02 kPa.

Implementation in COMSOL Multiphysics®

The model described above can straightforwardly be implemented in COMSOL Multiphysics® (COMSOL Multiphysics GmbH, Göttingen, Germany). The software enables the numerical solution of a large number of partial differential equations among which is the one given above. Besides, rotationally symmetric problems can be treated.

RESULTS AND DISCUSSION

Computer-aided modelling and simulation were used to analyse how adjustments in the concentration and oxygen affinity of Hb affect the oxyregulatory capacity of the water flea *D. magna*. The analyses were performed for two different cases. The Hb-poor low-affinity (PL) case was characterized by a Hb concentration (C_{Hb}) of 0.1 $mmol\,l^{-1}$ haem and a half-saturation oxygen tension (P_{50}) of 1.01 kPa simulating the oxygen transport in a normoxia-acclimated animal. The Hb-rich high-affinity (RH) case (C_{Hb}=0.5 $mmol\,l^{-1}$ haem, P_{50}=0.35 kPa) referred to the situation in a hypoxia-acclimated animal. For model validation, we compared the model predictions concerning (i) the dependence of oxygen consumption rate on inspiratory oxygen partial pressure (P_i), (ii) the contribution of Hb to circulatory oxygen transport, and (iii) the oxygen partial pressure distribution with experimental data. As a key parameter for comparison of oxyregulatory capacities, we used the critical P_i at which the overall oxygen consumption rate of the model decreased to 90% of its maximum. The results of all three validations are described below. A sensitivity analysis was then performed to determine how uncertainties in model parameters translate into variations in the critical P_i. Based on these plausibility checks, we finally estimated the advantage of oxygen-affinity changes in the *D. magna* Hb *via* a cost–benefit analysis.

Dependence of overall consumption rate on ambient oxygen tension

Our first validation comprised the simulation of steady-state oxygen supply and consumption for inspiratory oxygen tensions (P_i) ranging from normoxic values (20 kPa) to anoxic values (0 kPa). The simulation was carried out for the PL case (Fig. 2A) and the RH case (Fig. 2B). The progressive reduction in P_i from 20 kPa to about 7 kPa had almost no effect on the oxygen uptake rate (Fig. 2, solid lines), which remained virtually constant at a high level. With further reduction of P_i, however, the transport systems failed to supply enough oxygen to the tissues, and the overall consumption and uptake rate decreased more or less linearly with P_i. The critical P_i at which the consumption rate decreased to 90% of the maximum

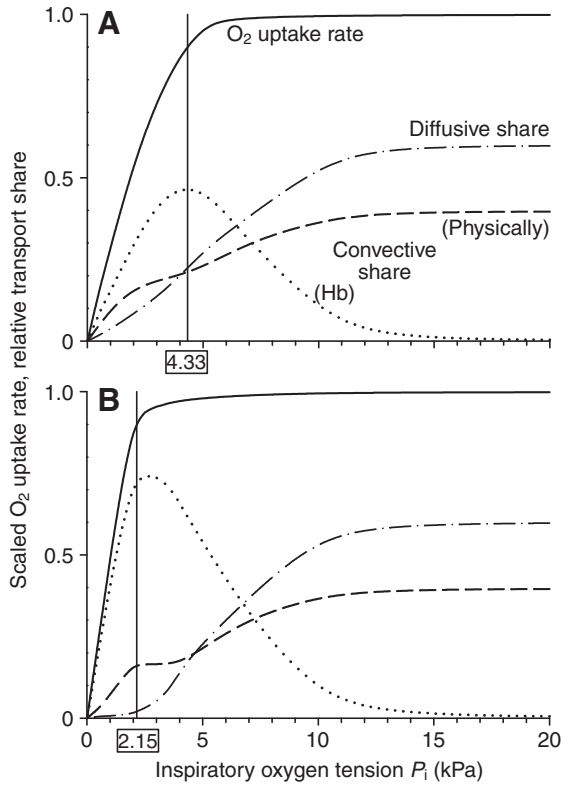

Fig. 2. Predicted dependence of oxygen consumption rate (solid lines) on ambient oxygen tension for the Hb-poor low-affinity case (A) and the Hb-rich high-affinity case (B). The vertical lines and adjacent numbers indicate the critical ambient oxygen tension at which the overall oxygen consumption rate decreased to 90% of the maximum. The other lines show the relative diffusive and convective share of tissue O_2 supply including those fractions which are transported by Hb and as physically dissolved portions.

was 4.33 kPa in the PL case and 2.15 kPa the RH case. Experimental values of 4.3±0.6 kPa (mean ± s.d.) for normoxia-acclimated animals and 2.0±1.0 kPa for hypoxia-acclimated animals were determined in a previous study (Seidl et al., 2005), which, however, defined the critical inspiratory value less strictly as 'the critical ambient oxygen tension at which the oxygen consumption rate started to decrease over-proportionally'. In spite of the difficulty in comparing these differently defined critical values, we consider the predictions on the general dependence of overall consumption rate on P_i to be in reasonable agreement with the experimental data.

Contribution of Hb to circulatory oxygen transport

Conceptually, the 'flow' of oxygen from the respiratory surfaces to the tissues can be divided into circulatory and non-circulatory subflow or share. The non-circulatory share refers to the oxygen molecules that diffuse across the trunk integument into the peripheral and adjacent tissue layers. The circulatory share describes the convective transport of the physically dissolved and Hb-bound oxygen forms in the haemolymph. Our second model validation compared the predictions on the magnitude of these different transport shares with published data. The convective transport of physically dissolved oxygen was determined by multiplying the ('arterial-to-venous') difference in the dissolved oxygen concentrations at the two virtual confluence points by total perfusion rate (Fig. 3A, open and filled circles). This approximation agrees with the chosen boundary conditions. The convective transport of the Hb-bound oxygen was quantified analogously. The difference between the overall oxygen consumption rate and the sum of convective (physically dissolved and Hb-bound) oxygen transport in the haemolymph yielded the non-circulatory diffusive share.

The non-circulatory (diffusive) share was 50–60% for both Hb cases and P_i values of 10–20 kPa (Fig. 2). The magnitude of this share is consistent with predictions from previous modelling and experimental studies (Pirow, 2003; Pirow et al., 2004; Pirow and Buchen, 2004). It shows that more than 50% of the oxygen molecules that are taken up per unit time interval at the respiratory surfaces do not follow the pathway predetermined by the circulating fluid. Instead, these oxygen molecules diffuse along steep, radial gradients from the trunk cuticle *via* the haemolymph to the adjacent tissue layers. Such radial oxygen gradients are not well established in the spatial oxygen profiles depicted in Fig. 3 (due to the lower P_i values) but have been documented elsewhere [see figure 8 of Pirow and Buchen (Pirow and Buchen, 2004)]. The diffusive share decreased more or less linearly with P_i for P_i values lower than 10 kPa.

The convective transport of the physically dissolved oxygen essentially showed the same dependence on P_i as the diffusive share (Fig. 2). In contrast, the relative contribution of Hb to convective oxygen transport was essentially zero at normoxic P_i values (20 kPa) but increased with decreasing P_i up to a maximum of 4.3 kPa in the PL case (Fig. 2A) and 2.5 kPa in the RH case (Fig. 2B). The maximum contribution of Hb to circulatory oxygen transport was 46% in the PL case and 74% in the RH case. The predicted dependence of Hb-mediated oxygen transport on P_i is consistent in qualitative terms with the experimental data on the depression of oxygen uptake following the poisoning of Hb with carbon monoxide (Hoshi and Yajima, 1970) [see figure 2 of Weber and Vinogradov (Weber and Vinogradov, 2001)].

Given the predicted absence of Hb-mediated oxygen transport under normoxia (Fig. 2), which is in line with experimental data (Hoshi and Yajima, 1970) [see figure 2 of Weber and Vinogradov (Weber and Vinogradov, 2001)], one may wonder why *D. magna* synthesizes a certain low amount of Hb under these conditions. As argued previously (Weber and Vinogradov, 2001), the 'apparent superfluousness (of Hb) under a given set of conditions does not exclude a vital role under another more stressful one'. The chosen parameterization of our model refers to a well-defined physiological condition (maximum activation of ventilatory and circulatory systems, fasting state, no eggs and embryos in the brood chamber) for which a broad spectrum of experimental data is available. There are indeed more stressful, physiologically challenging conditions for a water flea such as the period of brood release and carapace shedding at the end of the reproduction/moulting cycle. This period is characterized by a stereotypic motor behaviour (strong truncal and postabdominal flexions) and includes phases of ventilatory arrest. The metabolic perturbations developing during these apnoetic events have not been studied so far, but our model predictions (Fig. 4) show that even a low amount (0.1 mmol l^{-1}) of oxygenated Hb can act as a 'safety factor' (Weibel, 2000) as it substantially prolongs the time for maintaining oxygen consumption rate under these apnoetic conditions.

Spatial distribution of oxygen partial pressure

The oxygen partial pressure distribution in the cross-sectional plane of the radially symmetric body (Fig. 1C) was predicted for the PL case (Fig. 3A) and RH case (Fig. 3B). The inspiratory oxygen tension (P_i) was set to the critical level of 4.33 kPa and 2.15 kPa, respectively,

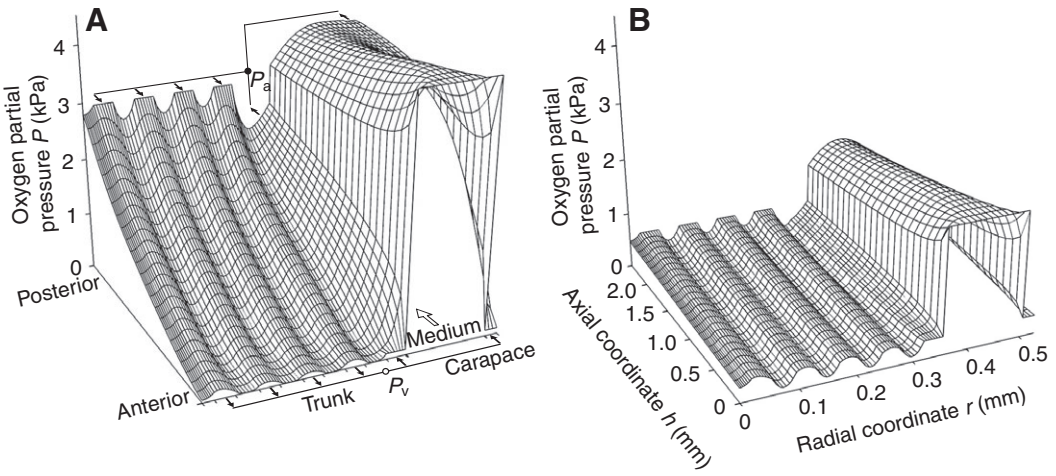

Fig. 3. Oxygen partial pressure distributions in the median plane of the radially symmetric model (see Fig. 1C) for the Hb-poor low-affinity case (A) and the Hb-rich high-affinity case (B). The distributions were calculated for an inspiratory oxygen partial pressure (P_i) of 4.33 kPa (A) and 2.15 kPa (B). The P_i values corresponded to the critical ambient oxygen tension at which the overall oxygen consumption rate of the model decreased to 90% of the maximum rate. Black and white arrows show the direction of the haemolymph and medium flow. P_a and P_v represent the arterial and venous oxygen tension at the posterior and anterior confluence points (open and filled circles).

at which the overall oxygen consumption rate of the model decreased to 90% of its maximum. The case-specific settings for the P_i and the Hb-related parameters lead to pronounced differences in the elevation of two-dimensional profiles and in the steepness of the anterior-to-posterior gradient (Fig. 3). These general characteristics are in line with experimental data on the oxygen partial pressure distributions in the circulatory system of normoxia-acclimated and hypoxia-acclimated animals under critical ambient oxygen conditions (Pirow et al., 2004). In the following sections, we will describe how the predicted oxygen profiles are generated by the underlying transport and consumption processes.

In each profile, the highest oxygen tensions occur in the medium, which flows through the space between the trunk and the carapace in a posterior direction. In the PL case (Fig. 3A), the medium oxygen tension decreases from 4.33 kPa (inspiratory value, P_i) at the anterior position to 3.69 kPa (mean expiratory value, P_e) at the posterior position, since oxygen diffuses along steep gradients into the adjacent haemolymph compartments of the carapace and the trunk. Oxygen-poor haemolymph enters these compartments at the anterior position and flows in a posterior direction. Due to the uptake of oxygen, the haemolymph oxygen tension increases to 3.77 kPa in the carapace lacuna and to 2.24 kPa in the peripheral trunk lacuna. The two currents join at the posterior confluence point where perfect mixing results in a mean oxygen tension of 2.92 kPa (arterial value, P_a). The oxygen saturation of Hb at this P_a is 89% (Fig. 5A, open circle). The oxygenated haemolymph then enters the trunk in four separate streams (Fig. 3A). Due to the release of oxygen into the adjacent tissue layers, the haemolymph oxygen tension decreases progressively until the low level of 0.1 kPa (venous value, P_v) is reached at the anterior position. Likewise, the oxygen saturation of Hb is reduced to 7% when the P_v value is reached (Fig. 5A, filled circle). The diffusive release of oxygen results in a wavy distribution of oxygen partial pressure with higher values in the haemolymph compartments and lower values in the tissue compartments. The four streams of oxygen-poor haemolymph leaving the trunk are finally re-combined at the anterior confluence point, and the circulation cycle starts again.

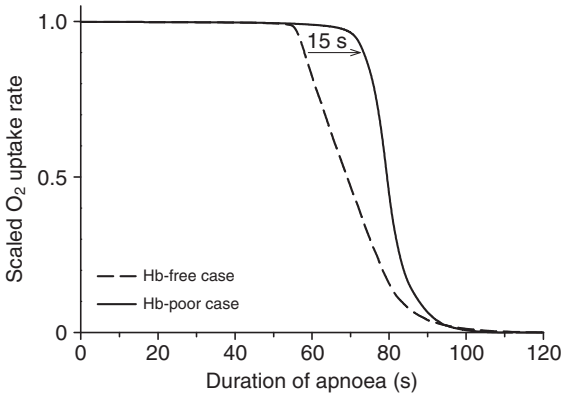

Fig. 4. Benefit of Hb under normoxic conditions. Shown is the predicted dependence of oxygen consumption rate on the duration of apnoea for a Hb-free case (dashed line) and the Hb-poor low-affinity case (solid line). During apnoetic events, the Hb-bound oxygen prolongs the time for maintaining oxygen consumption rate from 58 s to 73 s (gain in time: 25%). These times refer to a fasting animal with no eggs or embryos in the brood chamber. Much shorter times would occur in the presence of additional oxygen-consuming processes associated with the digestion of food or the respiratory activity of the brood.

An inspiratory oxygen tension of 4.33 kPa is required in the PL case to meet 90% of the overall oxygen demand. In the RH case (Fig. 3B), a much lower inspiratory value of 2.15 kPa (P_i) is sufficient to ensure the same percentage of oxygen provision. The mean expiratory value is 1.51 kPa (P_e). As in the PL case, the difference between the inspiratory and expiratory oxygen tensions is 0.74 kPa. However, the oxygen tensions in the haemolymph are confined to the narrow range between 0.31 and 0.82 kPa. The lower value represents the venous oxygen tension (P_v), the upper value is reached in the haemolymph leaving the carapace lacuna. The mean oxygen tension of the haemolymph leaving the peripheral trunk lacuna is 0.42 kPa. The mixing of the two haemolymph currents at the posterior confluence point results in an intermediate oxygen tension of 0.56 kPa (P_a), which is the maximum oxygen tension

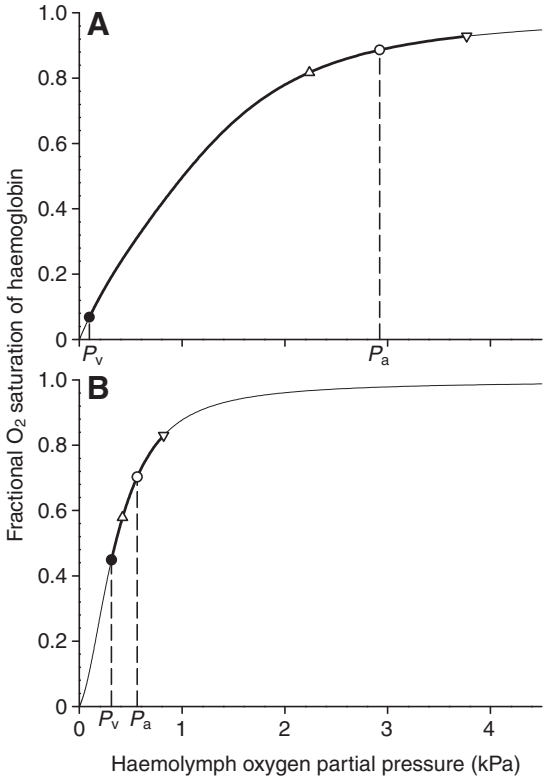

Fig. 5. Hb oxygen saturation in the haemolymph for the Hb-poor low-affinity case (A) and the Hb-rich high-affinity case (B) at the critical inspiratory oxygen tension of 4.33 kPa and 2.15 kPa, respectively. The thick solid lines indicate that part of the oxygen equilibrium curve that is used for the dynamic loading and unloading of oxygen. The open and filled circles represent the saturation at arterial (P_a) and venous oxygen tensions (P_v). The saturation values of the haemolymph leaving the carapace lacuna and the peripheral trunk lacuna are shown by the up and down triangles. Oxygen equilibrium curves were calculated according to Eqns 4 and 5 using reported Adair constants for the Hb of normoxia-acclimated and hypoxia-acclimated animals of *D. magna* (Kobayashi et al., 1994).

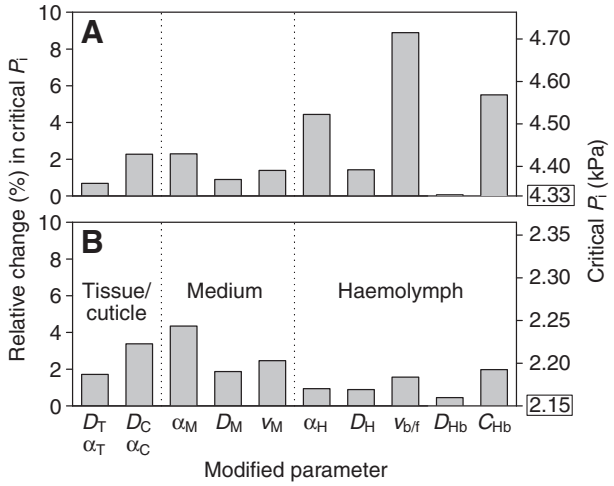

Fig. 6. Sensitivity analysis showing the relative increase in the critical inspiratory oxygen tension (P_i) by a 10% reduction in a single conductance parameter for the Hb-poor low-affinity case (A) and the Hb-rich high-affinity case (B). The critical P_i is additionally given in absolute values (right axis) including the reference levels (4.33 and 2.15 kPa). The tested parameters are listed along the horizontal axis. They comprise oxygen diffusion coefficients (D), oxygen solubility coefficients (α), flow velocities (v), and the Hb concentration (C_{Hb}). The different subscripts refer to the tissue, cuticle, medium and haemolymph compartments, and backward/forward direction.

experienced by the tissue. During the passage of haemolymph through the trunk, the Hb oxygen saturation decreases moderately from 70% to 45% (Fig. 5B, open and filled circles).

Sensitivity analysis

The modelled critical P_i values of normoxia-acclimated and hypoxia-acclimated animals indicate an appropriate parameterization. The chosen parameter values are based on experimental data but contain uncertainties. A common way to evaluate the effect of these uncertainties is to determine how a slightly altered parameterization translates into an altered model prediction. We analysed its sensitivity with respect to the standard parameterization used in the spatial analysis for the two cases separately. We altered individual parameter values one by one by ±10% while keeping all remaining parameters fixed to standard. As increase and reduction lead to comparable results opposite in sign only, we limit our subsequent discussion to the effects of a reduction.

Reducing transport-related parameters by 10% increased the critical P_i by 0.1–8.9% in the PL case (Fig. 6A) and by 0.5–4.3% in the RH case (Fig. 6B). In the PL case, the critical P_i was highly sensitive to changes in haemolymph flow velocity (v_b and v_f), Hb concentration (C_{Hb}), and the solubility for oxygen in haemolymph (α_H). The RH case showed the highest sensitivity to changes in the solubility for oxygen in the medium (α_M), the medium flow velocity (v_M), and the diffusion and solubility coefficients for oxygen in the cuticle (D_C and α_C).

The analysis of structural parameter changes was not as straightforward as that of functional adjustments, because any geometrical variation affects the overall parameterization when keeping the model constraints satisfied (see Materials and methods). We therefore simulated the 10% reduction in structural conductance parameters such as tissue/cuticle thickness by introducing an anisotropic diffusion coefficient where the diffusion of oxygen in the radial direction is scaled by the factor 1/0.9. In the PL case, the simulated reduction in tissue thickness and cuticle thickness decreased the critical P_i by 0.6% and 2.1%, respectively. Higher sensitivities (1.4% and 2.9%) were found for the RH case.

The analysis for consumption parameters revealed the highest sensitivity of the critical P_i to changes in the oxygen consumption rate (a_{max}) of tissue. The 10% reduction in a_{max} decreased the critical P_i by 13.5% in the PL case and by 10.4% in the RH case. In contrast, a 10% reduction in the oxygen partial pressure for half-maximum respiration (P_{50r}) decreased the critical P_i by only 0.4% in the PL case and by 1.4% in the RH case.

In addition to the analysis of conductance and consumption parameters, we tested whether neglecting fluid boundary layers in the medium and haemolymph compartments was justifiable. This test was accomplished by replacing the constant velocity profile (plug-flow) by a fully developed laminar parabolic velocity profile (see Appendix). Laminar flow conditions in the haemolymph compartments increased the critical P_i by only 0.8% in the PL case and by 2.3% in the RH case. In the medium compartment, the inclusion of fluid boundary layers increased the critical P_i by 3.2% in the PL case and by 8.8% in the RH case. Accordingly, neglecting fluid boundary layers was a reasonable model simplification for the haemolymph compartments but a critical simplification for the medium compartment.

The results of the sensitivity analyses have two important implications. From a validation perspective, it is clear that the more accurate the oxygen consumption rate, the flow velocities, and the solubility coefficients for oxygen in the haemolymph and medium, the more realistic the model predictions. From an analytic perspective, we can conclude that an effective oxyregulation under critical ambient oxygen conditions can be achieved, at least theoretically, by an adjustment of circulatory oxygen transport in the normoxia-acclimated animals and by a ventilatory change in the hypoxia-acclimated animals. The scope for a further enhancement of perfusion and ventilation is, however, essentially zero under critical ambient oxygen conditions since both systems already work at maximum rates. What is left under these conditions is either a metabolic depression or an adjustment in the concentration and/or oxygen affinity of Hb.

The advantage of affinity changes in Hb

The establishment and maintenance of a certain haemoglobin concentration is a considerable investment. Depending on the oxygen availability in the environment, the haemoglobin of *D. magna* can account for as much as 12% of the animal's dry weight (Kobayashi et al., 1988). By synthesizing Hb species of different oxygen affinities, *D. magna* might therefore follow a strategy to economize the amount of Hb needed to ensure an adequate oxygen supply. The use of high-affinity molecules in the hypoxia-exposed animals, for example, is supposed to reduce investment costs compared with the use of low-affinity molecules (Kobayashi et al., 1994; Paul et al., 2004). How great the economic advantage actually is, and under which environmental conditions and physiological states this economic advantage disappears, has remained unclear.

We applied our modelling approach to quantify the advantages and disadvantages achieved through the use of low-affinity Hb or high-affinity Hb. As in the simulations described in the previous sections, we considered two different Hb concentrations (0.1 mmol l^{-1} and 0.5 mmol l^{-1}) and a range of inspiratory oxygen tensions (P_i=0–8 kPa). For each combination of parameter values, we then calculated the steady-state oxygen distribution in the animal and determined the minimum oxygen partial pressure in the tissue. The latter value was used to derive the minimum oxygen consumption rate according to the Michaelis–Menten kinetics (last addend in Eqn 1). From a physiological point of view, it seems more important to ensure a minimum supply of oxygen to all parts of the body rather than an integral minimum provision over the whole body. We therefore used the local consumption rate of the 'worst-supplied' tissue region for evaluating supply performance. This criterion also conforms to a postulated oxyregulatory mechanism that activates Hb gene expression locally in the undersupplied tissue regions (Paul et al., 2004). Finally, for the less-well performing Hb type, we determined the extra amount of Hb needed to compensate for the lower supply performance.

Fig. 7A illustrates the supply performance of both Hb species in the case of low Hb concentration. As expected, the oxygen consumption rate of the worst-supplied tissue region increases with increasing P_i. However, this increase differs for the two Hb types, with the two curves intersecting at a P_i of 5.2 kPa. At lower P_i values, high-affinity Hb is more efficient than low-affinity Hb due to the steeper slope of the oxygen equilibrium curve in the lower range of haemolymph oxygen tension (Fig. 5B). This allows high-affinity Hb a higher degree of oxygen loading at the respiratory surfaces after reaching similar degrees of unloading in the haemolymph adjacent to the respective worst-supplied tissue region. At higher values of P_i, above 5.2 kPa, this 'loading advantage' diminishes, and the low-affinity Hb outdoes the high-affinity Hb due to an 'unloading advantage'. At the minimum oxygen tensions prevailing, the low-affinity Hb reaches a higher degree of unloading in the haemolymph due to the gentler slope of the oxygen equilibrium curve (Fig. 5A). Most of the behaviour of the curves is of rather theoretical interest because the Hb concentration chosen is too low to meet, for example, 80% of the oxygen demand (Fig. 7A, dotted line). We find that for any P_i value where this minimum is reached the low-affinity Hb guarantees a higher consumption rate than the high-affinity one. The costs of achieving the same level of oxygen provision with the high-affinity molecules are substantial. At a P_i of 6.1 kPa, for example, a 55% higher concentration of the high-affinity Hb would be required to raise the local consumption rate from 57% to the 85% level of the low-affinity Hb.

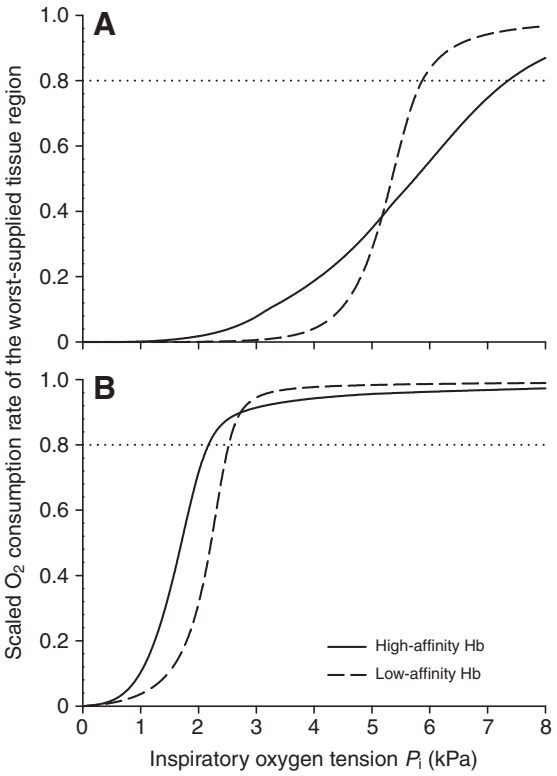

Fig. 7. Physiological advantage of using of high-affinity (solid lines) and low-affinity (dashed lines) Hb in the Hb-poor case (A) and in the Hb-rich case (B). The solid and dashed lines show the oxygen consumption rate of the worst-supplied tissue region dependent on the inspiratory oxygen tension (P_i).

Increasing the Hb concentration from 0.1 mmol l^{-1} to 0.5 mmol l^{-1} shifts both supply performance curves to the left (Fig. 7B); that is, they rise at smaller P_i values. The high-affinity Hb curve additionally shows a much steeper slope. As a consequence, the intersection of the two curves now appears at a smaller P_i (2.8 kPa) and at a higher consumption rate (90% of the maximum). The underlying mechanism for the differing supply performance of the two Hb species at P_i values above and below the intersection P_i is the same as for the low-Hb concentration case. Above the intersection P_i, however, the supply performance of the low-affinity Hb only slightly exceeds that of the high-affinity Hb, indicating that the former has essentially lost its unloading advantage. Below the intersection P_i, the high-affinity Hb clearly outdoes the low-affinity one in a physiologically sensible way. At a P_i of 2.3 kPa, for example, 85%

of the oxygen demand can be satisfied by the high-affinity type, but only 63% with the low-affinity one. To compensate for the lower supply performance of the low-affinity Hb, a 60% higher Hb concentration would be necessary.

Exchanging low-affinity Hb for high-affinity Hb turned out to be a mixed blessing for the animal. The benefit arising from the improved oxygen loading exceeds the disadvantage of impaired unloading only under conditions where the ambient oxygen tension is critically low and the Hb concentration is high. The low-affinity Hb, on the other hand, provides an advantage only if the Hb concentration is low and the ambient oxygen tension is well above the critical level. It should be noted that these general conclusions still hold for the reported variations in oxygen consumption rate such as the increase by 50% that follows the activation of digestive processes (Pirow and Buchen, 2004) and the decrease by 20% which follows the acclimation to hypoxic conditions (Seidl et al., 2005). These model-based findings now await an experimental verification which might be achieved through the microinjection of different Hb types into the circulatory system, followed by measurement of the tissue oxygenation state (using NADH fluorescence intensity) under different ambient oxygen tensions.

CONCLUSION AND PERSPECTIVES

Our approach to simulate the oxygen supply in *D. magna* allowed us to draw three main conclusions. Primarily we found that basic experimental results can be reproduced by a simplified numerical model. These simplifications comprise the description of transport processes through a classical convection–diffusion–reaction equation and the reduction of the animal's body to a series of concentric, hollow cylindrical compartments of tissue and haemolymph. Predictions were in reasonable agreement with the experimental data. Sensitivity analyses revealed fundamental differences in the oxyregulatory strategies between the two acclimation groups. Our ultimate goal was to quantify the advantage of maintaining two Hb types of different oxygen affinity. Assuming the objective to be a minimum oxygen supply to all parts of the animal's body, we found that the benefit arising from the improved oxygen loading of high-affinity Hb exceeds the disadvantage of impaired unloading only under conditions of critically low ambient oxygen tension and high Hb concentration.

Our spatio-temporally explicit integrative model showed its predictive advantages over local static molecular considerations as it reliably takes into account processes at the metabolic and systemic level. No single-level approach could have given, for example, a quantitative picture of the role of diffusive and convective processes, a well-founded explanation for the different oxyregulatory strategies, or ultimately a cost–benefit analysis of the affinity changes in the respiratory protein. Given sufficient experimental data one could even think of extending the dynamic character of the model through (i) the inclusion of feedback loops to control the Hb properties *via* synthesis/degradation processes, (ii) the consideration of kinetic aspects of the Hb oxygenation/deoxygenation reactions, or (iii) the integration of CO_2 transport and acid–base balance.

APPENDIX

The significance of fluid boundary layers in the medium and haemolymph compartments was tested by replacing the constant velocity profile (plug-flow) by a fully developed laminar parabolic velocity profile:

$$v(r) = \frac{\Delta p}{4\mu l}\left[r_o^2 - r^2 - \left(r_o^2 - r_i^2\right)\frac{\ln(r/r_o)}{\ln(r_i/r_o)}\right], \qquad \text{(A1)}$$

where r_i and r_o represent the inner and outer radii of the compartment in focus. The additional parameters are the compartment length l (mm), the pressure drop Δp (Pa) between the two compartment ends, and the dynamic viscosity μ (Pa s) of the fluid. The term $\Delta p/(4\mu l)$ was considered as a lumped parameter, and its value was derived from the radial extensions of and the plug-flow velocity u (=v_M, v_f or v_b) in the compartment under consideration:

$$\frac{\Delta p}{4\mu l} = \frac{2u}{r_o^2 + r_i^2 + (r_o^2 - r_i^2)/\ln(r_i/r_o)} \cdot \qquad \text{(A2)}$$

LIST OF SYMBOLS

a_{max}	O_2 consumption rate of tissue (nmol s^{-1} mm^{-3})
B	binding polynomial
C_{Hb}	haem-based Hb concentration (nmol mm^{-3})
D	diffusion coefficient for O_2 (mm^2 s^{-1})
D_C	diffusion coefficient for O_2 in cuticle (mm^2 s^{-1})
D_H	diffusion coefficient for O_2 in haemolymph (mm^2 s^{-1})
D_{Hb}	diffusion coefficient for Hb in haemolymph (mm^2 s^{-1})
D_M	diffusion coefficient for O_2 in medium (mm^2 s^{-1})
D_T	diffusion coefficient for O_2 in tissue (mm^2 s^{-1})
h	axial coordinate (mm)
K	Krogh constant for oxygen diffusion (nmol s^{-1} mm^{-1} kPa^{-1})
K_j	Adair constant of the jth binding step ($mmHg^{-1}$)
l	compartment length (mm)
$\dot{M}$	convective oxygen flux (nmol s^{-1})
N	number of interacting oxygen-binding sites
P	oxygen partial pressure (kPa)
P_{50}	half-saturation oxygen tension of Hb (kPa)
P_{50r}	oxygen tension for half-maximum respiration (kPa)
P_a	'arterial' oxygen tension (kPa)
P_e	expiratory oxygen tension (kPa)
P_i	inspiratory oxygen tension (kPa)
P_v	'venous' oxygen tension (kPa)
$\dot{Q}$	haemolymph flow rate (mm^3 s^{-1})
r	radial coordinate (mm)
r_i	inner radius of a hollow cylinder (mm)
r_o	outer radius of a hollow cylinder (mm)
S	fractional oxygen saturation
t	time (s)
u	plug-flow velocity (mm s^{-1})
v	axial velocity (mm s^{-1})
$\mathbf{v}$	vectorial velocity of convective flow (mm s^{-1})
v_b	haemolymph flow velocity in the backward direction (mm s^{-1})
v_f	haemolymph flow velocity in the forward direction (mm s^{-1})
v_M	medium flow velocity (mm s^{-1})
α_C	solubility coefficient for O_2 in cuticle (nmol mm^{-3} kPa^{-1})
α_H	solubility coefficient for O_2 in haemolymph (nmol mm^{-3} kPa^{-1})
α_M	solubility coefficient for O_2 in medium (nmol mm^{-3} kPa^{-1})
α_T	solubility coefficient for O_2 in tissue (nmol mm^{-3} kPa^{-1})
β	capacitance coefficient for O_2 (nmol mm^{-3} kPa^{-1})
Δp	pressure drop (Pa)
μ	dynamic viscosity (Pa s)

ACKNOWLEDGEMENTS

The authors wish to thank the DFG priority program Aquashift (SPP 1162) from which this cooperation emanated. It could not have succeeded otherwise.

REFERENCES

Binder, G. (1932). Das Muskelsystem von *Daphnia*. *Int. Rev. ges. Hydrobiol. Hydrog.* **26**, 54-111.

deFur, P. L., Mangum, C. P. and Reese, J. E. (1990). Respiratory responses of the blue crab *Callinectes sapidus* to long-term hypoxia. *Biol. Bull.* **178**, 46-54.

Eads, B. D., Andrews, J. and Colbourne, J. K. (2008). Ecological genomics in *Daphnia*: stress responses and environmental sex determination. *Heredity* **100**, 184-190.

Forstner, H. and Gnaiger, E. (1983). Calculation of equilibrium oxygen concentration. In *Polarographic Oxygen Sensors* (ed. E. Gnaiger and H. Forstner), pp. 321-333. Berlin: Springer-Verlag.

Fox, H. M. (1948). The haemoglobin of *Daphnia*. *Proc. R. Soc. Lond. Ser. B Biol. Sci.* **135**, 195-212.

Fox, H. M., Gilchrist, B. M. and Phear, E. A. (1951). Functions of haemoglobin in *Daphnia*. *Proc. R. Soc. Lond. B Biol. Sci.* **138**, 514-527.
Fryer, G. (1991). Functional morphology and the adaptive radiation of the Daphniidae (Branchipoda, Anomopoda). *Philos. Trans. R. Soc. Lond. B Biol. Sci.* **331**, 1-99.
Gnaiger, E., Steinlechner-Maran, R., Méndez, G., Eberl, T. and Margreiter, R. (1995). Control of mitochondrial and cellular respiration by oxygen. *J. Bioenerg. Biomembr.* **27**, 583-596.
Gnaiger, E., Lassnig, B., Kuznetsov, A., Rieger, G. and Margreiter, R. (1998). Mitochondrial oxygen affinity, respiratory flux control and excess capacity of cytochrome *c* oxidase. *J. Exp. Biol.* **201**, 1129-1139.
Gnaiger, E., Méndez, G. and Hand, S. C. (2000). High phosphorylation efficiency and depression of uncoupled respiration in mitochondria under hypoxia. *Proc. Natl. Acad. Sci. USA* **26**, 11080-11085.
Gorr, T. A., Cahn, J. D., Yamagata, H. and Bunn, H. F. (2004). Hypoxia-induced synthesis of hemoglobin in the crustacean *Daphnia magna* is hypoxia-inducible factor-dependent. *J. Biol. Chem.* **279**, 36038-36047.
Heckmann, L. H., Sibly, R. M., Connon, R., Hooper, H. L., Hutchinson, T. H., Maund, S. J., Hill, C. J., Bouetard, A. and Callaghan, A. (2008). Systems biology meets stress ecology: linking molecular and organismal stress responses in *Daphnia magna*. *Genome Biol.* **9**, R40.
Hoshi, T. and Yajima, T. (1970). Studies on physiology and ecology of plankton. XXIV. Possible role of blood haemoglobin induced by low oxygen culture in the respiration of *Daphnia magna*. *Sci. Rep. Niigata Univ. Ser. D Biol.* **7**, 107-115.
Imai, K. (1982). Allosteric effects in hemoglobin. Cambridge: Cambridge University Press.
Kimura, S., Tokishita, S., Ohta, T., Kobayashi, M. and Yamagata, H. (1999). Heterogeneity and differential expression under hypoxia of two-domain hemoglobin chains in the water flea, *Daphnia magna*. *J. Biol. Chem.* **274**, 10649-10653.
Kobayashi, M. (1983). Estimation of the haemolymph volume in *Daphnia magna* by haemoglobin determination. *Comp. Biochem. Physiol. A Physiol.* **76**, 803-805.
Kobayashi, M. and Hoshi, T. (1982). Relationship between the haemoglobin concentration of *Daphnia magna* and the ambient oxygen concentration. *Comp. Biochem. Physiol. A Physiol.* **72**, 247-249.
Kobayashi, M., Fujiki, M. and Suzuki, T. (1988). Variation in and oxygen-binding properties of *Daphnia magna* hemoglobin. *Physiol. Zool.* **61**, 415-419.
Kobayashi, M., Ishigaki, K., Kobayashi, M., Igarashi, Y. and Imai, K. (1994). Oxygen transport efficiency of multiple-component hemoglobin in *Daphnia magna*. *Can. J. Zool.* **72**, 2169-2171.
Krogh, A. (1919). The rate of diffusion of gases through animal tissue, with some remarks on the coefficient of invasion. *J. Physiol.* **52**, 391-408.
Lamkemeyer, T., Paul, R. J., Stöcker, W., Yiallouros, I. and Zeis, B. (2005). Macromolecular isoforms of *Daphnia magna* haemoglobin. *Biol. Chem.* **386**, 1087-1096.
Lamkemeyer, T., Zeis, B., Decker, H., Jaenicke, E., Waschbusch, D., Gebauer, W., Markl, J., Meissner, U., Rousselot, M., Zal, F. et al. (2006). Molecular mass of macromolecules and subunits and the quaternary structure of hemoglobin from the microcrustacean *Daphnia magna*. *FEBS J.* **273**, 3393-3410.
Paul, R. J., Colmorgen, M., Hüller, S., Tyroller, F. and Zinkler, D. (1997). Circulation and respiratory control in millimetre-sized animals (*Daphnia magna*, *Folsomia candida*) studied by optical methods. *J. Comp. Physiol. B Biochem. Syst. Environ. Physiol.* **167**, 399-408.
Paul, R. J., Zeis, B., Lamkemeyer, T., Seidl, M. and Pirow, R. (2004). Control of oxygen transport in the microcrustacean *Daphnia*: regulation of haemoglobin expression as central mechanism of adaptation to different oxygen and temperature conditions. *Acta Physiol. Scand.* **182**, 259-275.
Pirow, R. (2003). The contribution of hemoglobin to oxygen transport in the microcrustacean *Daphnia magna*-A conceptual approach. *Adv. Exp. Med. Biol.* **510**, 101-107.
Pirow, R. and Buchen, I. (2004). The dichotomous oxyregulatory behaviour of the planktonic crustacean *Daphnia magna*. *J. Exp. Biol.* **207**, 683-696.
Pirow, R., Wollinger, F. and Paul, R. J. (1999a). The sites of respiratory gas exchange in the planktonic crustacean *Daphnia magna*: An *in vivo* study employing blood haemoglobin as an internal oxygen probe. *J. Exp. Biol.* **202**, 3089-3099.
Pirow, R., Wollinger, F. and Paul, R. J. (1999b). The importance of the feeding current for oxygen uptake in the water flea *Daphnia magna*. *J. Exp. Biol.* **202**, 553-562.
Pirow, R., Bäumer, C. and Paul, R. J. (2004). Crater landscape: two-dimensional oxygen gradients in the circulatory system of the microcrustacean *Daphnia magna*. *J. Exp. Biol.* **207**, 4393-4405.
Poynton, H. C., Varshavsky, J. R., Chang, B., Cavigiolio, G., Chan, S., Holman, P. S., Loguinov, A. V., Bauer, D. J., Komachi, K., Theil, E. C. et al. (2007). *Daphnia magna* ecotoxicogenomics provides mechanistic insights into metal toxicity. *Environ. Sci. Technol.* **41**, 1044-1050.
Seidl, M. D., Paul, R. J. and Pirow, R. (2005). Effects of hypoxia acclimation on morpho-physiological traits over three generations of *Daphnia magna*. *J. Exp. Biol.* **208**, 2165-2175.
Shaw, J., Pfrender, M. E., Eads, B. D., Klaper, R., Callaghan, A., Colson, I., Gilbert, D. and Colbourne, J. K. (2008). *Daphnia* as an emerging model for toxicological genomics. In *Advances in Experimental Biology and Toxicogenomics* (ed. P. Kille and C. Hogstrand). Amsterdam: Elsevier.
Sugano, H. and Hoshi, T. (1971). Purification and properties of blood hemoglobin from fresh-water cladocera, *Moina macrocopa* and *Daphnia magna*. *Biochim. Biophys. Acta* **229**, 349-358.
Tokishita, S., Shiga, Y., Kimura, S., Ohta, T., Kobayashi, M., Hanazato, T. and Yamagata, H. (1997). Cloning and analysis of a cDNA encoding a two-domain hemoglobin chain from the water flea *Daphnia magna*. *Gene* **189**, 73-78.
Weber, R. E. and Vinogradov, S. N. (2001). Nonvertebrate hemoglobins: Functions and molecular adaptations. *Physiol. Rev.* **81**, 569-628.
Weibel, E. R. (2000). Symmorphosis: On form and function in shaping life. Cambridge, MA: Harvard University Press.
Zeis, B., Becher, B., Goldmann, T., Clark, R., Vollmer, E., Bölke, B., Bredebusch, I., Lamkemeyer, T., Pinkhaus, O., Pirow, R. et al. (2003). Differential haemoglobin gene expression in the crustacean *Daphnia magna* exposed to different oxygen partial pressures. *Biol. Chem.* **384**, 1133-1145.